J. Fluid Mech. (1984), *vol.* 139, *pp.* 67–95
Printed in Great Britain

The mixing layer: deterministic models of a turbulent flow. Part 2. The origin of the three-dimensional motion

By G. M. CORCOS AND S. J. LIN†
University of California, Berkeley, CA 94720

(Received 22 December 1982 and in revised form 9 August 1983)

Experimental evidence suggests that in the turbulent mixing layer the fundamental mechanism of growth is two-dimensional and little affected by the presence of vigorous three-dimensional motion. To quantify this apparent property and study the growth of streamwise vorticity, we write for the velocity field

$$V(x,t) = U(x,z,t)+u(x,y,z,t),$$

where U is two-dimensional and u is three-dimensional. In a first version of the problem U is independent of u, while in the second U is the spanwise average of V. In both cases the equation for u is linearized around U. The equations for U and u are solved simultaneously by a finite-difference calculation starting with a slightly disturbed parallel shear layer.

The solutions provide a detailed description of the growth of the three-dimensional motion. They show that its characteristics are dictated by the distribution of spanwise vorticity which results from roll-up and pairing. Pairing inhibits its growth. The solutions also demonstrate that even when the three-dimensional flow attains large amplitudes it has a negligible effect on the interaction of spanwise vortices and thus on the growth of the layer.

1. Introduction

In Part 1 (Corcos & Sherman 1984) we suggested that a comprehensive description of the turbulent shear layer might profitably be given by constructing first a deterministic prototype of the flow. Statistical properties of the real flow would then be obtained by averaging over a suitably chosen random superposition of such deterministic solutions.

To proceed this way downplays the dynamic importance of randomness and requires that the prototype exhibit essentially all the other properties of the real flow, including in particular both the range of lengthscales encountered in it and the ability which this flow shares with turbulence in general, greatly to enhance molecular diffusion. As is well known, both of these attributes are associated with the three-dimensionality of instantaneous realizations of turbulence and in particular with the effect in the vorticity equation of the term $(\boldsymbol{\Omega}\cdot\nabla)\boldsymbol{u}$ (where $\boldsymbol{\Omega}$ and $\boldsymbol{u}$ are the vorticity and velocity vectors).

Direct experimental evidence of the existence of non-planar components of the motion is of course also available, and in fact abounds, dating back to the original

† Present address: Scientific Research Associates, Glastonbury, Conn.

investigation of Liepman & Laufer (1949). But the nature of such motions is not easily inferred from the bulk of the measurements which have been made at one or two stationary points and which have been reduced to yield conventional statistical averages. For these see e.g. Wygnanski & Fiedler (1970). More recent experiments (Konrad 1977; Breidenthal 1981; Bernal 1981) have begun to suggest some of the features of the three-dimensional flow even though they, like their predecessors, have been hampered by the great difficulty inherent in capturing instantaneously panoramic realizations of dynamically significant quantities, such as the deformation rate and the vorticity. In fact, it is quite likely that the lack of a consensus on the presence (or absence) of a typical realization is due in large part to the uncertainty with which one has been able to relate dynamical properties which allow the motion to be inferred to those quantities like smoke (or visible products of diffusion-controlled reactions) whose instantaneous distribution one can record, at least in a plane.

Yet a theoretical study of the three-dimensional motion can profitably make use of some of our very fragmentary experimental knowledge. While in the initial unidirectional shear flow, it may be assumed that perturbations are generally three-dimensional, further downstream, as we have noted in Part 1, the instantaneous spanwise averages of large-scale features of a turbulent shear layer are remarkably similar to those of a strictly two-dimensional flow. This suggests that the environment in which the three-dimensional motion arises out of small perturbations is that described in Part 1. To ascribe a dominant and quasi-autonomous role to the two-dimensional motion is, at this stage, no more than a working hypothesis; but it can be subjected to a consistency check: it is part of the burden of a theoretical three-dimensional model based on it to demonstrate that the new motion does not destroy or seriously alter, but mostly accommodates itself to, the two-dimensional flow described in Part 1.

As mentioned there, the condition for this to be the case need not necessarily be that the amplitude of the three-dimensional motion be small. Nevertheless, it is instructive to study its dynamical origin by first assuming it small, as it must be initially, and by linearizing the equations describing its growth around the time-dependent nonlinear equation for the quasi-autonomous two-dimensional motion. Such an inquiry is related to, though distinct from, the classical infinitesimal stability theory whose application to the free shear layer we discuss now.

1.1. *Three-dimensional perturbations on a parallel shear flow*

This is the well-known theory (see e.g. Stuart 1963) for the second term in an expansion

$$\boldsymbol{q} = \boldsymbol{q}^{(0)} + \epsilon \boldsymbol{q}^{(1)} + \epsilon^2 \boldsymbol{q}^{(2)} + \ldots \quad \text{etc.} \tag{1.1}$$

of the velocity $\boldsymbol{q}$ (with a corresponding expansion for the pressure) in powers of the amplitude ϵ. The expansion generates a sequence of approximations to the Navier–Stokes equations, i.e.

$$\frac{\partial \boldsymbol{q}^{(n)}}{\partial t} + \rho^{-1} \nabla p^{(n)} - \nu \nabla^2 \boldsymbol{q}^{(n)} = -\sum_{r=0}^{n} (\boldsymbol{q}^{(n-r)} \cdot \nabla) \boldsymbol{q}^{(r)}, \tag{1.2}$$

where $n = 0, 1, \ldots$ etc., p is the pressure, ν the kinematic viscosity. $\boldsymbol{q}^{(0)}$ is the steady unidirectional flow $\boldsymbol{q}^{(0)} = \hat{\boldsymbol{e}}_x U_0(z)$. Since the solution for $\boldsymbol{q}^{(1)}$ will be used in §1.3 as the initial condition for another type of approximation, we review it here. x is the streamwise and y the spanwise coordinate, z is perpendicular to both. We now use the characteristic velocity $U_\infty = \lim_{z \to \infty} U_0(z)$ and length $\delta_1 = U_\infty (\partial U_0 / \partial y)^{-1}_{\max}$ to non-dimensionalize all quantities.

For $n = 1$, (1.2) admits solutions for $\boldsymbol{q}^{(1)}$ with components

$$\begin{pmatrix} u \\ v \\ w \end{pmatrix} = \begin{pmatrix} u_1 \\ v_1 \\ w_1 \end{pmatrix} \exp \mathrm{i}(\alpha x + \beta y - \alpha c t). \tag{1.3}$$

u_1, v_1, w_1 are functions of z, α and β are chosen real, while c is complex. If $m^2 = \alpha^2 + \beta^2$, u_1, v_1, w_1 are given by the eigensolutions of the linear equation

$$(U_0 - c)(w_1'' - m^2 w_1) - U_0'' w_1 = -\frac{\mathrm{i}}{\alpha R}(w_1'''' - 2m^2 w_1'' + m^4 w_1), \tag{1.4a}$$

together with the solutions of the non-homogeneous equation

$$(U_0 - c) g + \frac{\mathrm{i}}{\alpha R}(g'' - m^2 g) = w_1 U'. \tag{1.4b}$$

In (1.4) $R = U_\infty \delta_\mathrm{i}/\nu$, and w_1 and g are functions of the parameters m and αR and the variable z. In particular they are independent of the value of β/α for fixed values of m and αR. Primes denote differentiation with respect to z.

A composite solution describing waves standing in the spanwise direction can be constructed by taking the half-sum of the left-running $(+\beta)$ and right-running $(-\beta)$ solutions for u, v, w corresponding to a single solution of (1.4a, b). For such waves:

$$u = \frac{\mathrm{i}\alpha}{m^2} \cos \beta y \left[w_1' + \frac{\beta^2}{\alpha^2} g \right] \exp[\mathrm{i}\alpha(x - ct)], \tag{1.5a}$$

$$v = \frac{-\beta}{m^2} \sin \beta y [w_1' - g] \exp[\mathrm{i}\alpha(x - ct)], \tag{1.5b}$$

$$w = \cos \beta y \, w_1 \exp[\mathrm{i}\alpha(x - ct)]. \tag{1.5c}$$

For an appropriate range of m, solutions of the form assumed above grow in time. The non-dimensional growth rate has the form

$$\sigma \equiv \mathrm{Im}\left(\frac{\alpha c \delta}{U_0}\right) = \frac{\alpha}{m} G(m, \alpha R). \tag{1.6}$$

A plot of the function σ for an error-function profile $U_0(z)$ is given in figure 1 for $R = 50$ and 100 and $\alpha = 0.43$.

The significance of (1.6) is that, m remaining constant, and if we ignore the weak dependence of σ on the parameter αR when the latter exceeds say 50, the growth rate of a three-dimensional perturbation is smaller by the factor α/m than that of a two-dimensional perturbation ($\beta = 0$, $\alpha = m$). Now the growth rate σ of a planar disturbance is known to reach a maximum for a value of m such that $0 < m < 1$, and it is clear from (1.6) that no perturbation for which $\beta \neq 0$ can match this growth rate. Thus classical infinitesimal stability theory indicates that initially any three-dimensional perturbation grows less rapidly than some planar one. But this result soon contributes to the inadequacy for our purposes of the classical approach. For it implies that even before three-dimensional perturbations have grown sufficiently large to require a nonlinear description, the two-dimensional perturbations which have grown side by side with them, having grown faster, are likely to have seriously distorted the base flow around which the former were linearized. A modicum of progress can be made by solving for $\boldsymbol{q}^{(2)}$ in (1.2) as was done, in particular, by Benney (1961), who showed that this term in the expansion includes among other interactions that between two-dimensional and skewed waves. But the conclusions of such an

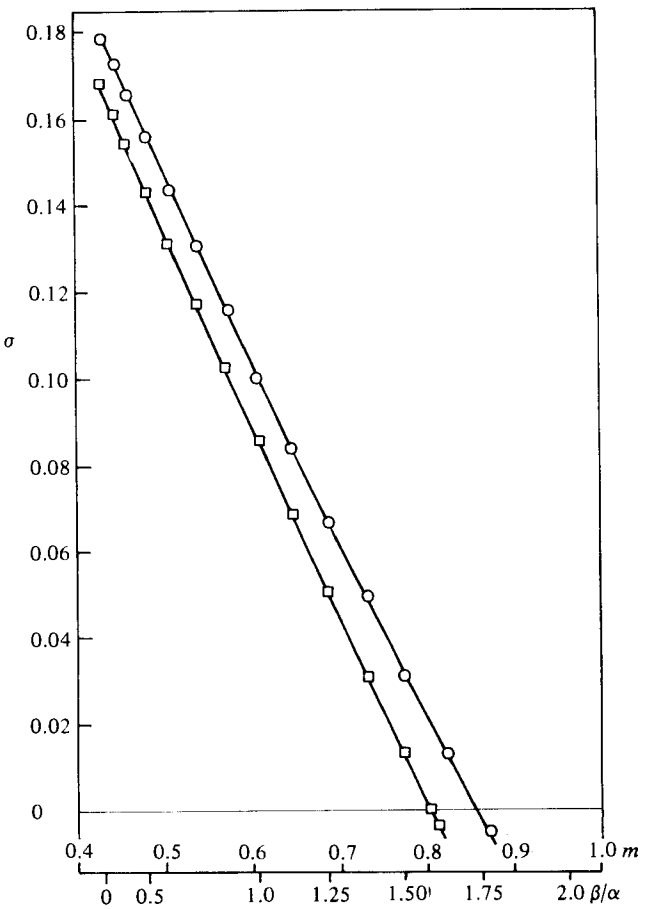

FIGURE 1. The initial growth rate σ of three-dimensional perturbations as a function of the spanwise wavenumber. The base flow is an error-function profile $U_0(Z)$, the streamwise wavenumber is $\alpha = 0.43$. □, $R = 50$; ○, $R = 100$.

analysis (Corcos 1979) are only suggestive of the later behaviour of the flow: the first two terms of the expansion can be a close approximation to the solution only for $\epsilon \ll 1$ (in which case the second-order term is a minor correction to the first), whereas, as shown in Part 1, perturbations of the original parallel flow acquire an amplitude of order unity in time of order $tU_0/\lambda \approx 1$, where $\lambda = 2\pi\delta_i/\alpha$.

1.2. *Three-dimensional perturbations on a row of diffuse vortices*

The inability of classical theory to account properly for the rapid evolution of the two-dimensional base flow to a state which is very different from the initial one has led Pierrehumbert & Widnall (1982) to study the three-dimensional instability of a steady flow of a different kind: an x-wise infinite row of diffuse vortices with vorticity distribution

$$\Omega = \frac{U_\infty k(1-A^2)}{(\cosh kz + A\cos kx)^2}, \tag{1.7}$$

where $0 \leqslant A \leqslant 1$. This distribution satisfies the steady Euler equations (Stuart 1967) and has been discussed in Part 1. Pierrehumbert & Widnall superpose on this flow infinitesimal and inviscid perturbations of the form

$$\phi(x,z)\exp[\sigma t + \mathrm{i}(\alpha x + \beta y)], \tag{1.8}$$

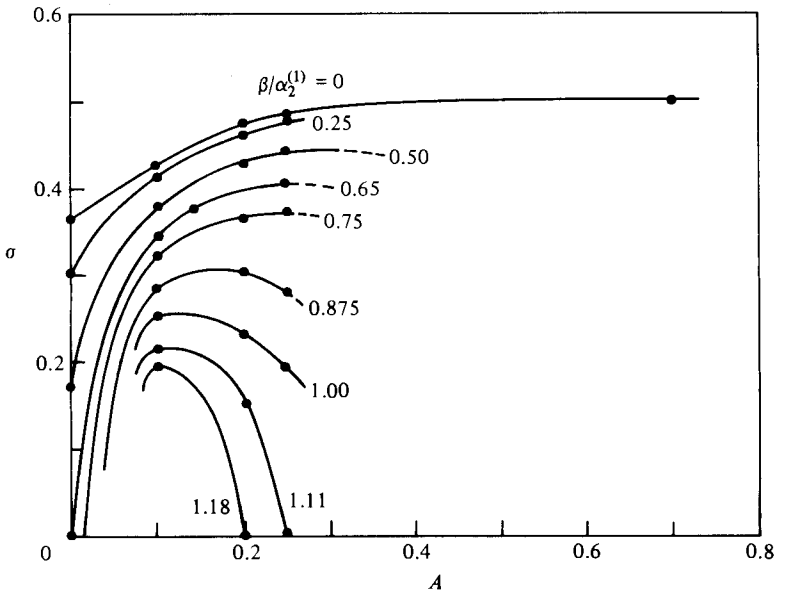

FIGURE 2. After Pierrehumbert & Widnall (1982): the initial growth rate σ of three-dimensional 'pairing' perturbations. The base flow is a row of Stuart vortices. The parameter A is a measure of the vortex concentration. The streamwise wavelength of the perturbation is twice the vortex spacing.

where α, β and σ are real. This leads to a two-dimensional eigenvalue problem for $\phi(x,t)$ which is solved numerically. The two main results reported by the authors are as follows.

(*a*) When $\alpha = \frac{1}{2}k$, i.e. for three-dimensional subharmonic instability, the growth rate has a maximum for $\beta = 0$ (two-dimensional case) and decreases rapidly as β increases. Figure 2 is a plot of the growth rate σ as a function of the two-dimensional vorticity concentration parameter A with the spanwise wavenumber β as a parameter. It shows that the value of σ drops rapidly as β increases especially beyond $\beta/\alpha = 1.0$ and for $A > 0.25$. Now $A = 0.25$ corresponds to rather diffuse vortices for which less than 59 % of the vorticity is found within the cat's-eyes and the cat's-eye semiheight is $0.177 \times 2\pi/k$. According to the results presented in Part 1, a value of A more typical of a rolled-up vorticity layer for $R \geqslant 50$ is $A = 0.6$, for which figure 2 suggests that only disturbances with long spanwise wavelengths have a growth rate at all comparable to the two-dimensional ones. Thus the initial instability associated with coalescence or pairing is preferentially two-dimensional, though pairing disturbances with spanwise wavelengths three or four times as large as the vortex spacing should be frequently seen according to this model.

(*b*) When the streamwise periodicity of the perturbation is imposed by the base flow ($\alpha = 0$) (so that all Stuart vortices are perturbed in identical fashion) the instability is necessarily three-dimensional: the perturbations are neutrally stable for $\beta = 0$. Their growth rate reaches a maximum for a value of the ratio β/k which increases with the value of the concentration parameter A. But the growth rate decreases only gradually as the spanwise wavenumber increases beyond the optimum value for growth. This mode of instability thus allows perturbations to grow on concentrated vortices even when the perturbation spanwise wavelength is too short to allow growth on a parallel shear layer. Pierrehumbert & Widnall termed this new instability translative and suggested that it is responsible for the spanwise oscillations

and streamwise streaks of visible reaction products in Breidenthal's (1981) experiments with a mixing layer.

These results are new and informative. The identification of an instability that is quite distinct both from the Orr–Sommerfeld and from the pairing kind is particularly significant. But it is difficult to infer from them with confidence how small three-dimensional perturbations evolve in the shear layer. The difficulty is the same as that discussed earlier in connection with the classical analysis of parallel shear flow: there is no justification for assuming that the base flow is steady, since the characteristic timescale for its own instability is at least initially shorter than that of the three-dimensional instability. Thus the limitations inherent in the linearized analysis of perturbations are here also compounded by an unrealistic assumption about the flow which gives rise to the instability considered. More specifically, we note the following.

(i) It is not clear how the modes discovered by the authors are related in time to the growing modes given by the classical theory which must be relevant at an earlier stage of the layer evolution.

(ii) The assumed vorticity distribution of the model base flow is substantially different from that which develops from the initial-value problem of the two-dimensional shear layer, especially at large Reynolds numbers. This can be seen by comparing the results of Part 1 with (1.7) above: the Stuart vortices are symmetric with respect to both midplanes $x = 0$ and $z = 0$, while the rolled-up mixing layer is a row of vorticity spirals with only point symmetry; for the instability described under (*b*), coalescence, a major redistribution of the spanwise vorticity of the base flow is ignored.

(iii) Finally, the assumption of a steady base flow implies an exponential or at least a monotonic growth or decay rate for linearized perturbations, whereas comparison of the two eigenvalue problems (§§1.1 and 1.2), each one with a different steady base flow leads to the inference that, as the base flow evolves, some perturbations which were initially stable become unstable so that conversely some others which are found unstable in such an analysis may well become stable at some later stage of the evolution of the base flow.

2. An alternative approach

An approach which avoids the difficulties mentioned above, which is consistent with the point of view developed in §1 and which is computationally as economical as that followed by Pierrehumbert & Widnall is as follows.

2.1. *The model*

If $\boldsymbol{V}$ and $\boldsymbol{\Pi}$ are the velocity vector and the pressure respectively, we split them as follows:

$$\boldsymbol{V}(x,y,z,t) = \boldsymbol{U}(x,z,t) + \boldsymbol{u}(x,y,z,t), \tag{2.1a}$$

$$\boldsymbol{\Pi}(x,y,z,t) = P(x,z,t) + p(x,y,z,t), \tag{2.1b}$$

where $\boldsymbol{U} = \hat{\boldsymbol{e}}_x U + \hat{\boldsymbol{e}}_z W$ is alternatively the solution of two differential equations in two versions of the flow. The first is

$$\boldsymbol{U}_t + (\boldsymbol{U}\cdot\boldsymbol{\nabla})\,\boldsymbol{U} + \rho^{-1}\boldsymbol{\nabla}P = \nu\boldsymbol{\nabla}^2\boldsymbol{U}, \tag{2.2a}$$

and the second is

$$\boldsymbol{U}_t + (\boldsymbol{U}\cdot\boldsymbol{\nabla})\,\boldsymbol{U} + \rho^{-1}\boldsymbol{\nabla}P - \nu\boldsymbol{\nabla}^2\boldsymbol{U} = -\frac{1}{L}\int_{y_0}^{y_0+L} (\boldsymbol{u}\cdot\boldsymbol{\nabla})\,\boldsymbol{u}\,\mathrm{d}y, \tag{2.2b}$$

where L is a suitable interval defined later. According to (2.2a) $\boldsymbol{U}$ is given independently of the coexistence of the three-dimensional field $\boldsymbol{u}$, while according to (2.2b) $\boldsymbol{U}$ is the spanwise average of the total velocity vector $\boldsymbol{V}$. In both cases the three-dimensional part of the velocity, i.e. $\boldsymbol{u} = \hat{\boldsymbol{e}}_x u + \hat{\boldsymbol{e}}_y v + \hat{\boldsymbol{e}}_z w$ satisfies

$$\boldsymbol{u}_t + (\boldsymbol{u}\cdot\boldsymbol{\nabla})\,\boldsymbol{U} + (\boldsymbol{U}\cdot\boldsymbol{\nabla})\,\boldsymbol{u} + \rho^{-1}\boldsymbol{\nabla}p = \nu\nabla^2\boldsymbol{u}, \tag{2.3}$$

an approximation to the exact equation for $\boldsymbol{u}$ obtained from the Navier–Stokes equation for $\boldsymbol{V}$ after splitting according to (2.1) by linearizing $\boldsymbol{u}$ around the time- and space-dependent two-dimensional field $\boldsymbol{U}$.

It follows from the linearity of (3.3) that if $\boldsymbol{u}$ and p are represented by Fourier series or integrals in the spanwise variable y, no interaction takes place between the Fourier components so that each component can be solved independently. Thus if

$$\left.\begin{aligned} &u = \hat{u}(x,z,t)\cos\beta y, \quad v = \hat{v}(x,z,t)\sin\beta y, \quad w = \hat{w}(x,z,t)\cos\beta y,\\ &p = \hat{p}(x,z,t)\cos\beta y \end{aligned}\right\} \tag{2.4}$$

(in which case $L = 2\pi/\beta$ in (2.2b)), (2.3) involves only the two space variables x and z and the parameter β. Then the complexity of the joint solution of (2.2a or b) and (2.3) is numerically comparable to that for the two-dimensional problem (2.2) alone, the number of numerical operations required being roughly doubled.

The right-hand side of (2.2b), with $L = 2\pi/\beta$ is obtained directly at every time step from the solution of (2.3) at the previous time step.

The numerical scheme is that used in Part 1. The grid has 64 mesh points in the x-direction and 81 in the z-direction over an interval = 1.25 × the grid length.

A comparison of the solutions of system (2.2a), (2.3) with those of system (2.2b), (2.3) yields a direct evaluation of the effect of the three-dimensional motion on the spanwise-averaged properties of the layer and also reveals whether the evolution of the three-dimensional flow is substantially different when the two- and three-dimensional motions are coupled.

2.2. *Initial conditions*

The initial values for $\boldsymbol{U}$ and $\boldsymbol{u}$ describe the superposition of

(a) a parallel flow

$$\boldsymbol{U}_0 = \hat{\boldsymbol{e}}_x\, U_\infty \operatorname{erf}\left(\frac{\pi^{\frac{1}{2}}z}{2\delta_i}\right),$$

the result of the viscous diffusion of a uniform vortex sheet;

(b) eigensolutions of the linearized form of (2.2a) with $\boldsymbol{U} = \hat{\boldsymbol{e}}_x\, U_0(z)$as in Part 1, i.e. solutions of (1.4a) with $m = \alpha_2$, $\beta = 0$;

(c) eigensolutions of (1.4a, b) with $U = U_0(z)$, $\alpha = \alpha_3$, $\beta \neq 0$.

The required eigensolutions are generated by an efficient algorithm which is incorporated in the program but for which the vertical range $z_{\min} \leqslant z \leqslant z_{\max}$ is divided into 600 intervals.

2.3. *Boundary conditions*

These are periodic in x (over a length that is the smallest common multiple of $2\pi/\alpha_2$ and $2\pi/\alpha_3$), periodic in y (with $v = 0$ on $y = \pm n\pi/\beta$, $n = 0, 1, 2, \ldots$ etc.) and such that $\boldsymbol{u}$ and $\boldsymbol{U} \mp \hat{\boldsymbol{e}}_x U_\infty \to 0$ as $z \to \pm\infty$. Since the last conditions are in fact imposed at $z = \pm z_{\max}$ (as though there were two conveyor belts there), they do not exclude the occasional generation of very weak boundary layers in the immediate neighbourhood of the upper and lower margins of the grid.

Case	R	$\alpha_2^{(1)}$	$\alpha_2^{(2)}$	α_3	$\frac{\beta}{\alpha_3}$	$\left\|\frac{\hat{w}}{\hat{W}}\right\|_0$	Equations used
1	50	0.43	—	0.43	1.25	$\frac{1}{3}$	(2.2a) and (2.3)
2	50	0.43	—	0.43	0.50	$\frac{1}{3}$	(2.2a) and (2.3)
3	50	0.43	—	0.43	0.90	$\frac{1}{3}$	(2.2a) and (2.3)
4	50	0.43	—	0.43	1.59	$\frac{1}{3}$	(2.2a) and (2.3)
5a	100	0.43	—	0.43	1.25	$\frac{1}{3}$	(2.2a) and (2.3)
5	50	0.43	0.215	0.215	1.73	$\frac{1}{3}$	(2.2a) and (2.3)
6	50	0.43	0.215	0.215	0.5	$\frac{1}{3}$	(2.2a) and (2.3)
7	50	0.43	0.215	0.43	0.50	$\frac{1}{3}$	(2.2a) and (2.3)
8	50	0.43	0.215	0.43	1.25	$\frac{1}{3}$	(2.2a) and (2.3)
9	50	0.43	0.215	0.43	0.50	$\frac{1}{3}$	(2.2b) and (2.3)
10	50	0.43	0.215	0.43	0.50	1	(2.2b) and (2.3)

TABLE 1

2.4. *Parameters*

These include α_2, α_3, β, R and the amplitudes of all the initial eigenfunctions.

For the two-dimensional flow $\boldsymbol{U}$, if a single periodic perturbation is introduced initially, $\alpha_2 = 0.43$, which corresponds approximately to the fastest initial growth for the assumed initial profile. This condition allows only growth and roll-up of the base flow. When two planar perturbations are introduced initially, we have chosen $\alpha_2^{(1)} = 0.43$ and $\alpha_2^{(2)} = 0.215$. The presence of the first subharmonic $\alpha_2^{(2)}$ allows one pairing or coalescence to occur after roll-up (see Part 1).

For the three-dimensional flow $\boldsymbol{u}$, the streamwise wavenumber α_3 was chosen equal to $\alpha_2^{(1)}$ or to $\alpha_2^{(2)}$. $R = 50$ for all runs. This was judged after some experimentation (case 5a) to be the largest acceptable Reynolds number for the mesh size used. Solutions were calculated for a range of values of β. The initial amplitudes were small enough for the numerical solutions to reproduce for early times the growth rate of Orr–Sommerfeld theory, though larger than might be achieved experimentally near the origin of a mixed layer issued from the merger of two quiet streams with laminar boundary layers on the upstream splitter plate. A typical value of the maximum root-mean-square amplitude of the initial fluctuation is $u' = 10^{-2}\Delta U$, where $\Delta U = 2U_\infty$. For U, whenever two initial values of α_2 were used, the amplitude of the subharmonic was half that of the fundamental. For the three-dimensional velocity $\boldsymbol{u}$, $|\hat{w}| = a|W|$, where $a = \frac{1}{3}$ or 1.

The reference velocity and length used to non-dimensionalize all variables are U_∞ and $\lambda = 2\pi/\alpha_2^{(1)}$. Thus non-dimensional time $\tau = tU_\infty/\lambda$. Since for all cases $\alpha_2^{(1)} = \alpha_2 = 0.43$, $\lambda = 14.6\delta_i$ and the grid area is either 1×1.25 (cases 1, 2, 3, 4, 5a) or 2×2.50 (cases 5, 6, 7, 8, 9, 10). Table 1 identifies the cases that were calculated.

2.5. *Results for an independent base flow*

We now discuss joint solutions of (2.2a) and (2.3) (cases 1–8) for which the base flow $\boldsymbol{U}$ is independent of $\boldsymbol{u}$.

2.5.1. *The energetics of the three-dimensional motion*

We define the local kinetic-energy density of the base flow as

$$e_2 = \frac{(U-\bar{U})^2 + W^2}{2U_\infty^2},$$

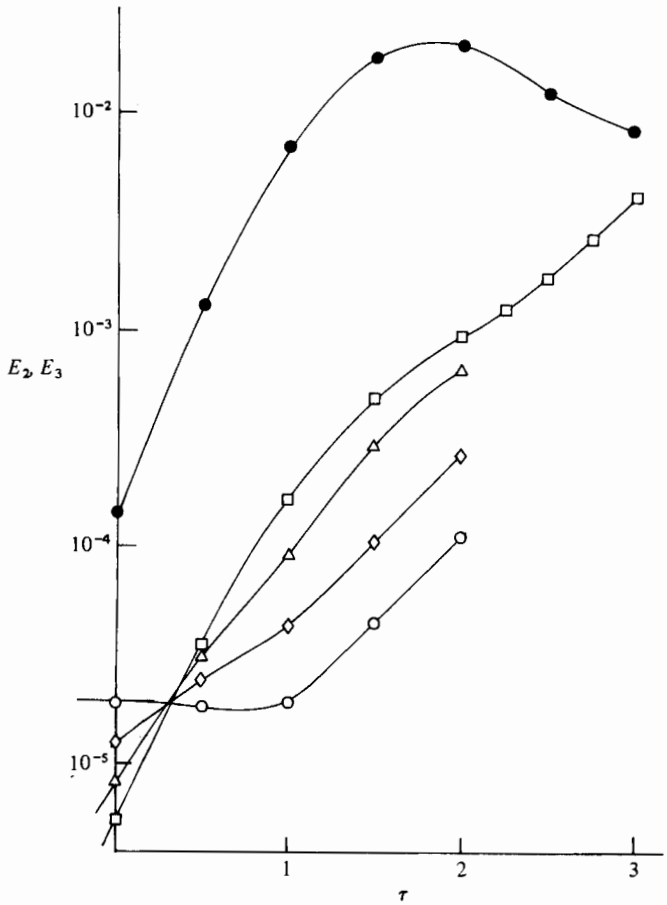

FIGURE 3. The kinetic energy of the base flow $\boldsymbol{U}$ and of the three-dimensional perturbation $\boldsymbol{u}$ as functions of time. The initial two-dimensional perturbation is a single wave. The base flow (●) is independent of $\boldsymbol{u}$ and the same for all cases. For $\boldsymbol{u}$: ◇, case 1; □, 2; △, 3; ○, 4 (see table 1). Indicated slopes at $\tau = 0$ from Orr–Sommerfeld theory.

where $\overline{U}(z,\tau)$ is the average of U over the length of the grid. The spanwise average of the kinetic energy density associated with the three-dimensional component $\boldsymbol{u}$ of $\boldsymbol{V}$ is

$$\tfrac{1}{2}e_3 = \frac{1}{4U_\infty^2}\{\hat{u}^2+\hat{v}^2+\hat{w}^2\}.$$

The integrals of e_2 and $\frac{1}{2}e_3$ over the grid are $E_2(\tau)$ and $E_3(\tau)$. The spanwise average of the local rate at which kinetic energy is transferred from the base flow to $\boldsymbol{u}$ is given by

$$\tfrac{1}{2}p_{\mathrm{r}} = \frac{1}{2}\left\{(\hat{u}^2-\hat{w}^2)\frac{\partial U}{\partial x}+\hat{u}\hat{w}\left(\frac{\partial U}{\partial z}+\frac{\partial W}{\partial x}\right)\right\}.$$

The integral of $\frac{1}{2}p_{\mathrm{r}}$ is P_{r}.

Figure 3 plots E_2 and E_3 as functions of time for cases 1–4 (roll-up). The initial growth rate agrees well with that given by Orr–Sommerfeld theory (indicated as a slope at $\tau = 0$). According to the latter, with $\alpha_3 = 0.43$ and $R = 50$, $\beta/\alpha = 1.59$ (case 4) corresponds to a neutrally stable wave. Initially, as is clear from both the calculations and Orr–Sommerfeld theory, the growth rate increases monotonically as β/α decreases. But, as the two-dimensional flow evolves, the character of the

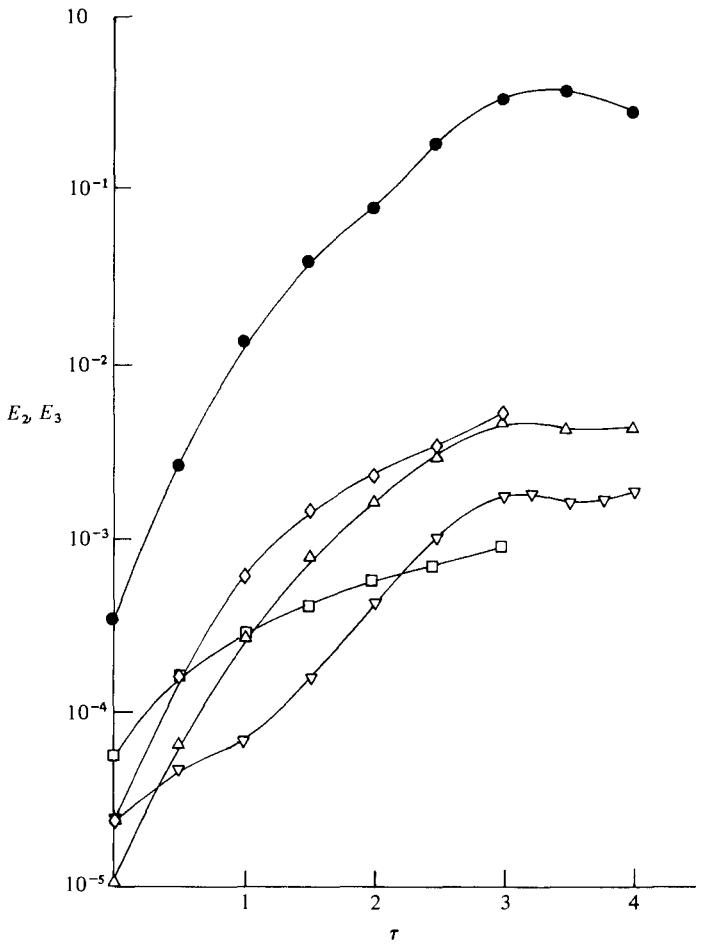

FIGURE 4. The kinetic energy of the base flow $\boldsymbol{U}$ and of the three-dimensional perturbation $\boldsymbol{u}$ as functions of time. The initial two-dimensional perturbation is the sum of a wave and its subharmonic. The base flow (●) is independent of $\boldsymbol{u}$ and the same for all cases. For $\boldsymbol{u}$: □, case 5; ◇, 6; △, 7; ▽, 8 (see table 1).

two-dimensional instability evidently changes: the growth rate for small spanwise wavenumbers decreases somewhat while that for the larger values of β increases. At $\tau \approx 1.5$ the growth rate is about the same for all values of β chosen ($0.5 \leqslant \beta \leqslant 1.59$), including that for the initially stable wave.

This result is qualitatively consistent with that of Pierrehumbert & Widnall (1981) for the translative instability. During the late stages of the roll-up of the base flow ($\tau > 2.0$) and in the absence of a subharmonic perturbation, the kinetic energy of that motion ceases to increase (for a discussion see e.g. Corcos & Sherman 1976), but the growth of the three-dimensional perturbation continues at about the same rate. This is additional evidence that the nature of the three-dimensional instability has been modified by the evolution of the base flow.

In figure 4 the same quantities are plotted, but the base flow is allowed to roll up and to pair once. As a result the kinetic energy of the base flow continues to increase until coalescence has occurred ($\tau = 3.5$). Here we note that coalescence has a striking effect on the instability of the three-dimensional motion. This is readily apparent on

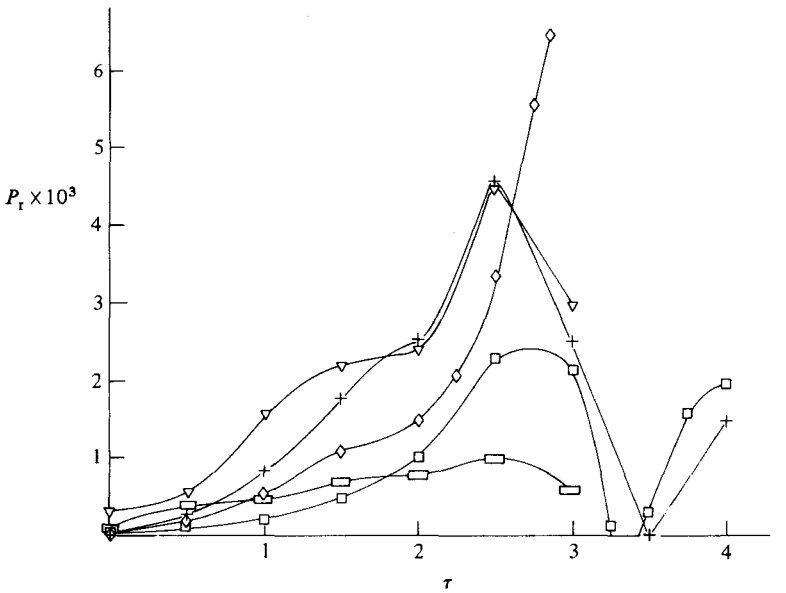

FIGURE 5. The rate of transfer of kinetic energy from $\boldsymbol{U}$ to $\boldsymbol{u}$. Roll-up and pairing cases: ▭, 5; ▽, 6; +, 7; □, 8; ◇, roll-up only, case 2 (see table 1).

figure 4 for the two calculations ($\beta/\alpha = 0.5$; $\beta/\alpha = 1.25$) which we carried out till $\tau = 4.0$. The cause of this temporary stabilization of $\boldsymbol{u}$ can be traced to a radical decrease in the net energy extracted by the Reynolds stress of the three-dimensional motion from the base flow. Figure 5 shows that in all cases involving pairing (unlike case 2 shown for comparison), this energy production P_r drops precipitously beyond $\tau = 2.5$, i.e. as the two primary spanwise vortices rotate around and press against each other.

In summary, roll-up, i.e. the concentration of spanwise vorticity into a regular array of diffuse vortices, gives rise to a new instability which allows shorter spanwise perturbations to grow in such a way that all the vortices are identically distorted, but coalescence, which rotates these vortices around each other and modulates their separation distance, halts this instability at least temporarily.

2.5.2. *The local evolution*

The transition from parallel-shear-flow instability to translative instability and the effect of coalescence on the latter are readily apparent from the evolution of the field values of e_3 and p_r. Quantities displayed at $\tau = 0$ are always calculated directly from the eigenfunctions for the parallel flow. For the roll-up we use case 2 ($\beta/\alpha_3 = 0.5$) as an example. Contours of constant values of e_3 in the (x, z)-plane are shown on figures 6 (a, b) for $\tau = 0$ and $\tau = 2.0$, together with a map of contours of the spanwise vorticity Ω of the base flow at $\tau = 2.0$. The periodic pattern associated with the weak vorticity wave at $\tau = 0$ has evolved in such a way that where Ω is small (left and right margins), the kinetic energy associated with $\boldsymbol{u}$ is also small. High values of e_3 are found only at the centre of the spanwise vortex. Note also a slight ridge of kinetic energy along the direction of principal axes of positive strain rate issuing from left and right stagnation points. These are associated with the very localized, quasi-unidirectional intense vorticity found in these regions (see figure 11 b). Figures 7 (a, b) show contours of production rate for the same case. These also become strongly centred on the inner

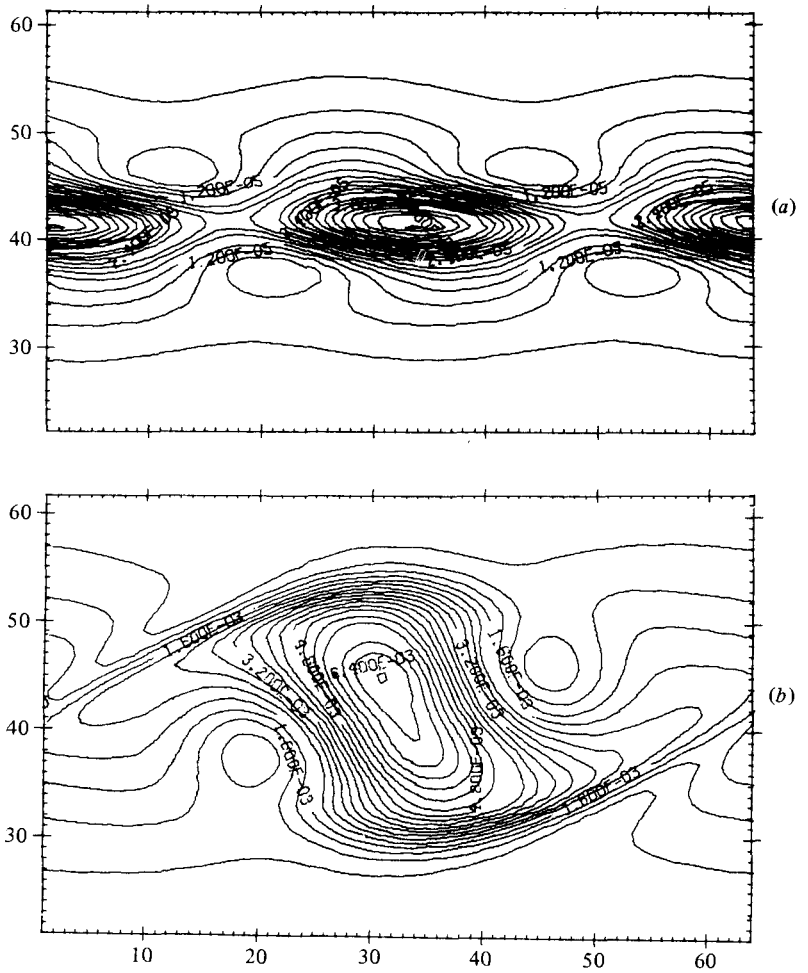

FIGURE 6(a, b). For caption see facing page.

part of the spanwise vortex core. This suggests that the translative instability is an instability of the vortex core.

While the maps of e_3 and p_r depend in their details on the value of β/α_3, they all exhibit the features described here.

For the roll-up and coalescence, we use case 7 and show e_3 and p_r at $\tau = 0$, 2.0 and 3.0 in figures 8(a–c) and 9(a–c). Here again, the centres of kinetic energy and of production rate of this energy faithfully follow the two spanwise vortices. It is also clear that as the braids become more completely depleted of spanwise vorticity (figure 14b) very little of the kinetic energy of the three-dimensional motion is produced there.

The effect of pairing on the new instability is striking in figure 10 (case 8, $\tau = 3.25$); weak production persists in the braids but the whole core has been temporarily stabilized so that, within it, production is negative. At later times production is renewed, but it has not reached its former level at the end of the computation ($\tau = 4$), at which time a second pairing would be occurring (see Part 1) if a second subharmonic perturbation $\alpha_2^{(3)}$ were present.

When the value of α_3 is equal to that of the subharmonic $\alpha_2^{(2)}$ as in cases 5 and 6, the streamwise periodicity of the fundamental $\alpha_2^{(1)}$ is rapidly impressed on the longer

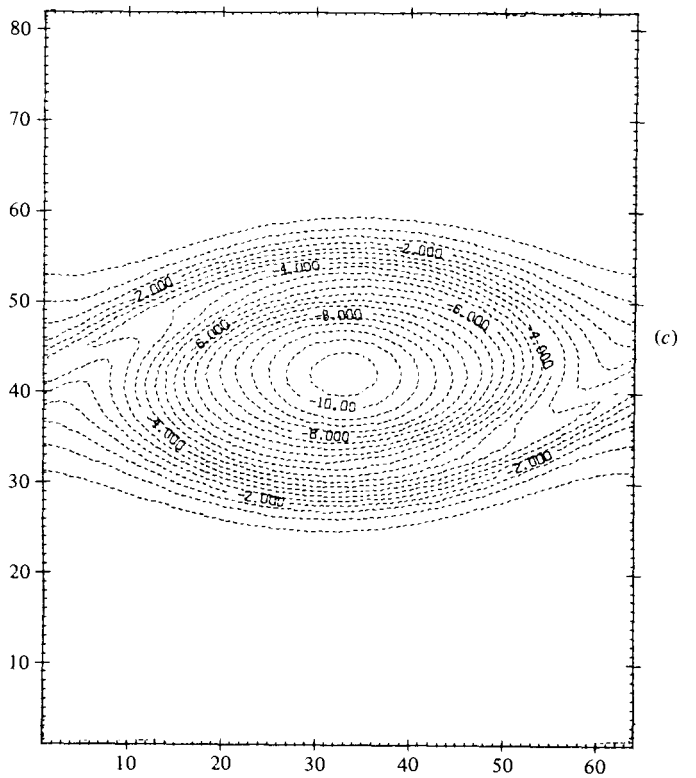

FIGURE 6. The local kinetic energy associated with $\boldsymbol{u}$ during roll-up (case 2). Contours of constant value in the (x, z)-plane: (*a*) $\tau = 0$; (*b*) $\tau = 2.0$. Contours of constant value of the vorticity associated with $\boldsymbol{U}$ at $\tau = 2.0$ are shown on (*c*).

three-dimensional perturbation, so that, around $\tau = 2.0$, the latter almost appears as if the value of its initial streamwise wavenumber were that of the fundamental. Later, its history through pairing is not notably different from that of the other cases. Thus cases 5 and 6, which might have been expected to resemble the cases of helical pairing instability calculated by Pierrehumbert & Widnall (1982) are in fact quite different.

3. The nature of the vorticity field

Let

$$\boldsymbol{\nabla} \times \boldsymbol{U} \equiv \boldsymbol{\Omega} \equiv \hat{\boldsymbol{e}}_y \Omega, \quad \boldsymbol{\nabla} \times \boldsymbol{u} \equiv \boldsymbol{\omega} \equiv \tilde{\boldsymbol{\omega}} + \hat{\boldsymbol{e}}_y \omega_2, \quad \boldsymbol{u} \equiv \tilde{\boldsymbol{u}} + \hat{\boldsymbol{e}}_y v,$$

where $\tilde{\boldsymbol{\omega}}$ and $\tilde{\boldsymbol{u}}$ are vectors in the (x, z)-plane and $\hat{\boldsymbol{e}}_y$ is the spanwise unit vector. We term $\tilde{\boldsymbol{\omega}}$ the streamwise vorticity.

The evolution equations for $\tilde{\boldsymbol{\omega}}$ and ω_2 which are consistent with (2.3) are

$$\left(\frac{\mathrm{D}}{\mathrm{D}t} - \nu\nabla^2\right)\tilde{\boldsymbol{\omega}} = \Omega \frac{\partial \tilde{\boldsymbol{u}}}{\partial y} + (\tilde{\boldsymbol{\omega}} \cdot \boldsymbol{\nabla})\, \boldsymbol{U}, \tag{3.1}$$

$$\left(\frac{\mathrm{D}}{\mathrm{D}t} - \nu\nabla^2\right)\omega_2 = -\tilde{\boldsymbol{u}} \cdot \boldsymbol{\nabla}\Omega + \Omega \frac{\partial v}{\partial y}, \tag{3.2}$$

where

$$\frac{\mathrm{D}}{\mathrm{D}t} = \frac{\partial}{\partial t} + \boldsymbol{U} \cdot \boldsymbol{\nabla}.$$

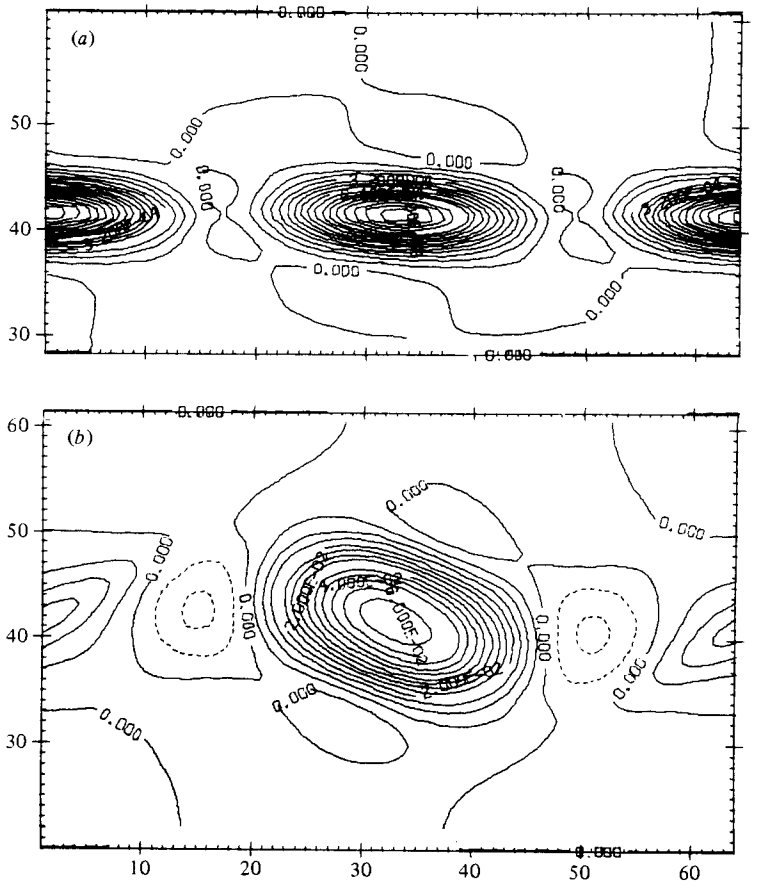

FIGURE 7. The local rate of transfer of kinetic energy from $\boldsymbol{U}$ to $\boldsymbol{u}$ during roll-up (case 2). Contours of constant value in the (x, z)-plane: (a) $\tau = 0$; (b) $\tau = 2.0$.

Let Γ be the circulation of $\boldsymbol{u}$ around a loop $\mathscr{C}$:

$$\Gamma \equiv \oint_{\mathscr{C}} \boldsymbol{u} \cdot \mathrm{d}\boldsymbol{s}.$$

Denote by $\mathrm{d}\Gamma/\mathrm{d}t$ the rate of change of Γ as the loop is advected by the base flow velocity $\boldsymbol{U}$. Then use of Stokes' theorem, (3.3) and a few tensor identities leads to

$$\frac{\mathrm{d}\Gamma}{\mathrm{d}t} = \iint_A \left[\Omega \frac{\partial \boldsymbol{u}}{\partial y} - \hat{\boldsymbol{e}}_y (\tilde{\boldsymbol{u}} \cdot \nabla \Omega) + \nu \nabla^2 \boldsymbol{\omega} \right] \cdot \boldsymbol{n} \, \mathrm{d}A, \tag{3.3}$$

where $\boldsymbol{n}$ is the unit normal to the element of surface $\mathrm{d}A$, and A is a surface bounded by $\mathscr{C}$.

Now choose the loop $\mathscr{C}$ so that it initially lies in a surface whose normal is everywhere perpendicular to the y-axis.

The loop will then remain at all times imbedded in such a surface according to our definition of $\mathrm{d}/\mathrm{d}t$ and ω_2 will not contribute to the circulation Γ_s around such a loop. We then get

$$\frac{\mathrm{d}\Gamma_s}{\mathrm{d}t} = \iint_A \left(\Omega \frac{\partial \tilde{\boldsymbol{u}}}{\partial y} + \nu \nabla^2 \tilde{\boldsymbol{\omega}} \right) \cdot \boldsymbol{n} \, \mathrm{d}A. \tag{3.4}$$

The sole source for this circulation associated with the streamwise vorticity $\tilde{\omega}$ is therefore $\Omega \, \partial \tilde{\boldsymbol{u}}/\partial y$. Hence this term may also be identified as the origin of the

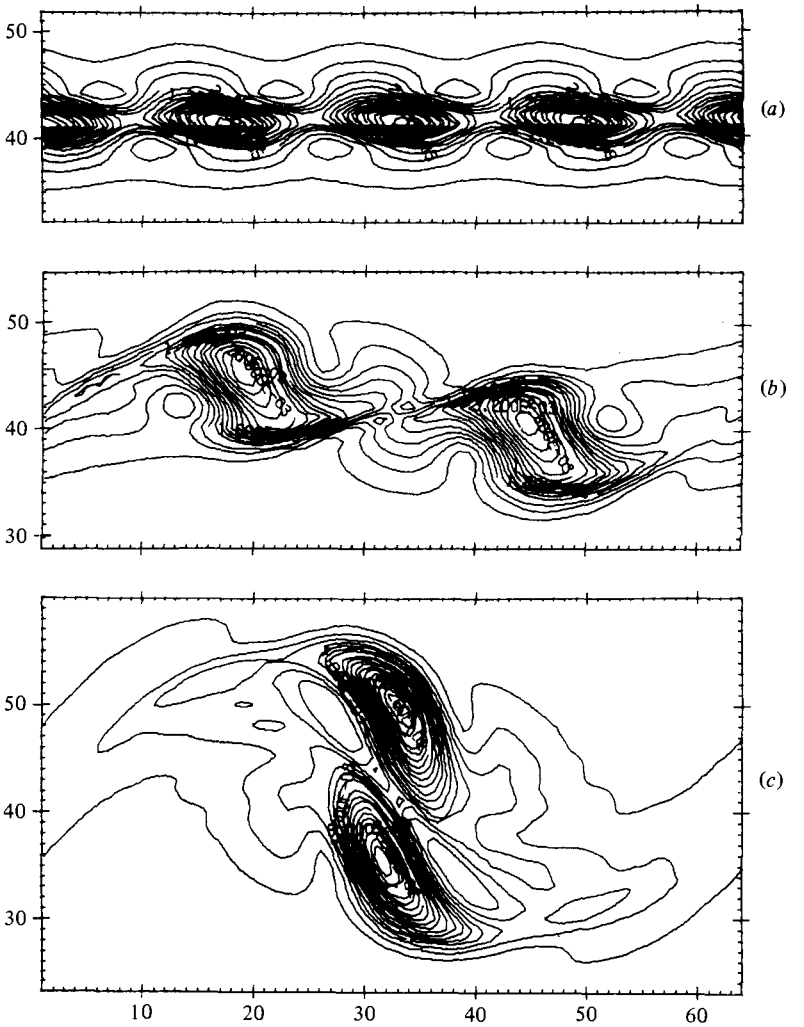

FIGURE 8. The local kinetic energy associated with $\boldsymbol{u}$ during roll-up and pairing (case 7). Contours of constant value in the (x, z)-plane: (*a*) $\tau = 0$; (*b*) 2.0; (*c*) 3.0.

streamwise vorticity in (3.1), while the second right-hand term enhances and redirects the streamwise vorticity already present, by means of the plane deformation of the base flow. In particular these equations indicate that streamwise vorticity cannot continue to be fed by interaction with the base flow wherever in the mixing layer the spanwise vorticity of that flow disappears. The streamwise vorticity that is created earlier in those regions, i.e. before the spanwise vorticity has migrated to the cores, may and does increase, but only as a result of the strain of the base flow and without change in circulation.

On the other hand, wherever, as in the rather large neighbourhood of the stagnation points, the direction of the (base-flow) strain field evolves only slowly, strain causes both ω_2 and the component of $\tilde{\boldsymbol{\omega}}$ normal to the axis of principal positive deformation to disappear as well as $\boldsymbol{\Omega}$; thus one should expect near the stagnation points essentially straight vortices of constant circulation lined up with the braids, as soon as these have been depleted of base-flow spanwise vorticity.

Figures 11 (*a*, *b*) show the distribution of streamwise vorticity $\tilde{\boldsymbol{\omega}}$ for case (2) at $\tau = 0$

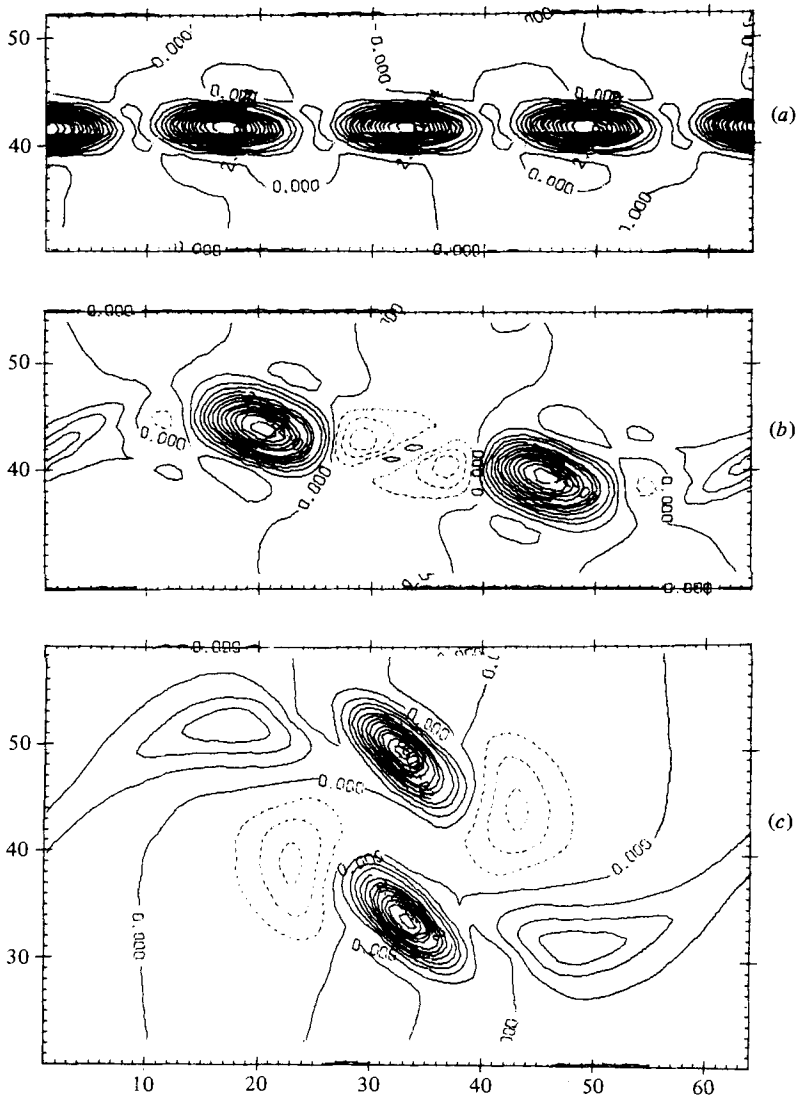

FIGURE 9. The local rate of transfer of kinetic energy from $\boldsymbol{U}$ to $\boldsymbol{u}$ during roll-up and pairing (case 7). Contours of constant value in the (x, z)-plane. (*a*) $\tau = 0$; (*b*) 2.0; (*c*) 3.0. For $\tau = 3.0$ the base-flow vorticity contours are shown on figure 14(*b*).

and at $\tau = 2$. $\tilde{\boldsymbol{\omega}}$ is depicted by an arrow whose length and tip size are proportional to $|\tilde{\boldsymbol{\omega}}|$. Contours of spanwise vorticity Ω at time $\tau = 2.0$ (figure 6*c*) do not exhibit well-formed braids, and a substantial amount of vorticity remains in the neighbourhood of the stagnation points. This is partly due to the low value of R in these calculations, but more to the fact that for roll-up, instability leads to braids only if $\alpha < 0.2$. This point is discussed in Corcos & Sherman (1976). Thus, in the present case, according to (3.4) the circulation of $\tilde{\boldsymbol{u}}$ around the stagnation points should continue to increase, and the calculations confirm this inference. Nevertheless the typical deformation field around the stagnation points (a saddle) is already well-established, since Ω has a strong maximum at the centre of figure 6(*c*) and the orientation of the streamwise vorticity near the stagnation points already coincides with the principal

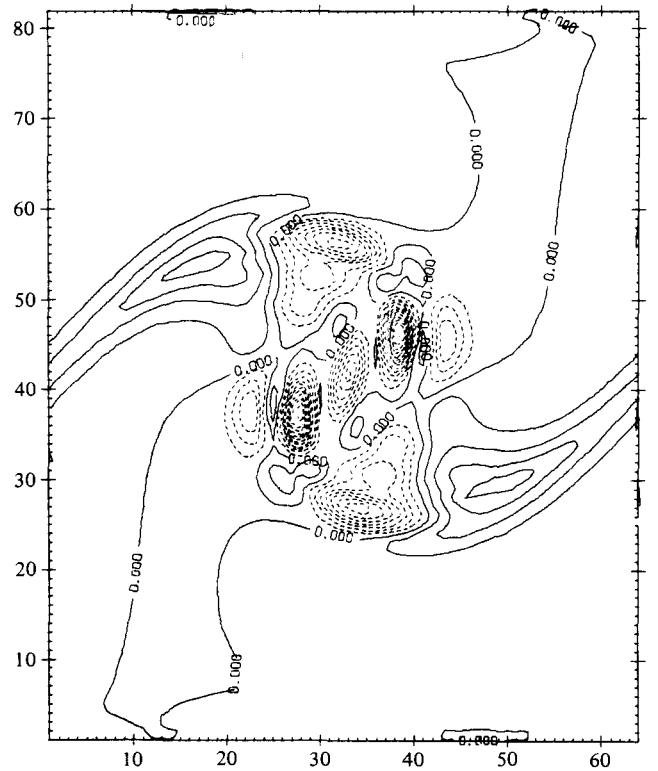

FIGURE 10. The effect of pairing on the translative instability: the local rate of transfer of kinetic energy from $\boldsymbol{U}$ to $\boldsymbol{u}$ during pairing; case 8, $\tau = 3.25$. Dotted contours denote negative rates.

axes of positive strain. Within the core one is struck by the uniformity of the orientation of $\tilde{\omega}$ which must be that of the principal axis of strain in that region.

The spanwise periodic pattern of ω_2 which modulates the distribution of Ω is shown on figure 12 for $\tau = 2.5$. This pattern is typical of all the roll-up cases studied. Near the stagnation point, ω_2 is quite small, as expected. Elsewhere the distribution is such as to displace the vorticity maximum either towards the backward or slow stream and upstream or towards the forward or faster stream and downstream. The displacement (figure 13) periodic in y and identical for the spanwise vortices is analogous to that found by Pierrehumbert & Widnall (1982) for the translative instability. This displacement vector of the vorticity maximum in the (x, z)-plane makes an angle with the x-axis which is found to increase with β/α_3.

When the base-flow evolution includes one pairing, the pattern of streamwise vorticity $\tilde{\omega}$ is more complex. The braids of the base flow are well-formed and narrow as soon as pairing occurs. Near the stagnation points, the direction of $\tilde{\omega}$ is accurately that of the braids, but within the cores streamwise vorticity appears folded several times. This reflects the more eventful evolution of the strain field created by the two precessing spanwise vortices of the base flow. Contours of constant magnitude of $\tilde{\omega}$ are shown for case (7) on figure 14(*a*) for $\tau = 3.0$, while figure 14(*b*) shows the distribution of Ω at the same time. Only a few arrows are shown on figure 14(*a*) for clarity. They indicate the direction and magnitude of streamwise vorticity at special points: (*a*) the stagnation points and the centre of symmetry of the picture, which are regions of minimum spanwise vorticity and very large strain; in both cases the

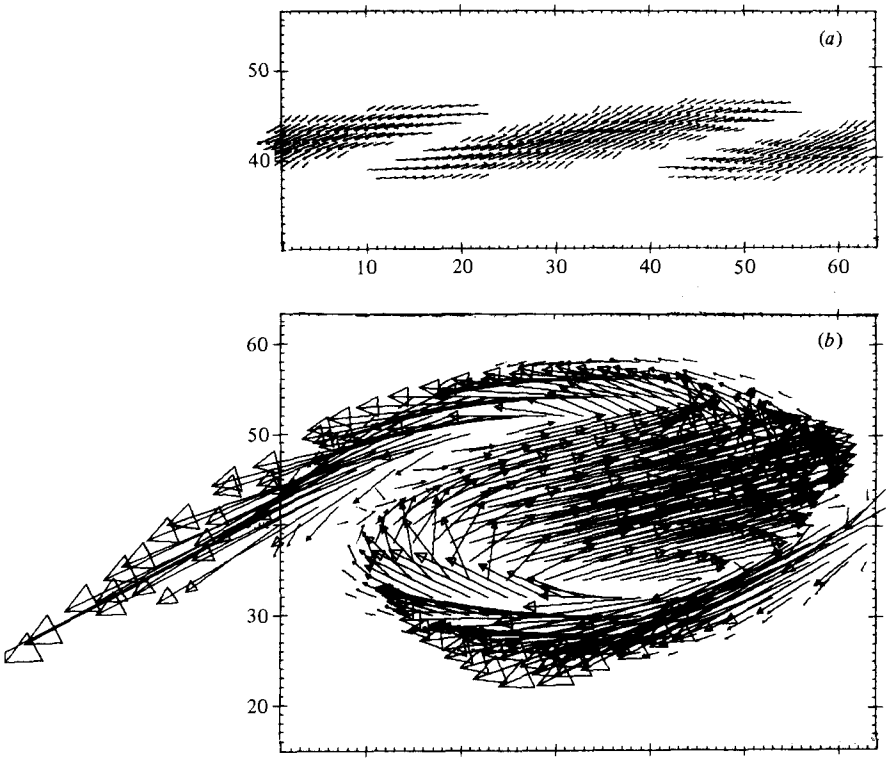

FIGURE 11. The projection $\tilde{\omega}$ of the vorticity $\nabla \times \boldsymbol{u}$ on to the (x, z)-plane; roll-up (case 2): (a) $\tau = 0$; (b) $\tau = 2.0$. The distribution of Ω at $\tau = 2.0$ is shown on figure 6(c).

vector $\tilde{\omega}$ is aligned with the direction of the principal (positive) strain; and (b) the centres of the two coalescing vortices, i.e. spanwise vorticity maxima where $\tilde{\omega}$ points approximately 45° from the direction of the prevailing principal strain axes in the core. The latter rotate in time with the two precessing spanwise vortices.

We note that, while the magnitude of $\tilde{\omega}$ is particularly large along the braids and at the two spanwise vortex centres, the thickness of the fluid layers which rotate coherently around axes in the (x, z)-plane is quite small. For the case at hand $(\beta/\alpha_3 = 0.5, \alpha_3 = \alpha_2^{(1)} = 0.43)$ this means that the streamwise vorticity occurs in thin layers elongated in the spanwise direction.† Within the braids there is only one such layer, but within the cores several layers are stacked and give rise to counterrotating flows.

4. The coupled case

So far, the base flow $\boldsymbol{U}(x, z, t)$ has been obtained by solving equation (2.2a), so that the three-dimensional field $\boldsymbol{u}$ was not allowed to influence its evolution. We now repeat some of these calculations but instead solve (2.2b) together with (2.3). This is done for two different initial amplitude ratios, $|\hat{w}|/|\hat{W}| = \frac{1}{3}$ (case 9) and $|\hat{w}|/|\hat{W}| = 1$ (case 10). The results for both $\boldsymbol{U}$ and $\boldsymbol{u}$ can then be compared with those for case 7, which is otherwise identical, but for which $\boldsymbol{U}$ is independent of $\boldsymbol{u}$.

† Part 3 (Lin & Corcos 1984) studies the nonlinear evolution of similar layers.

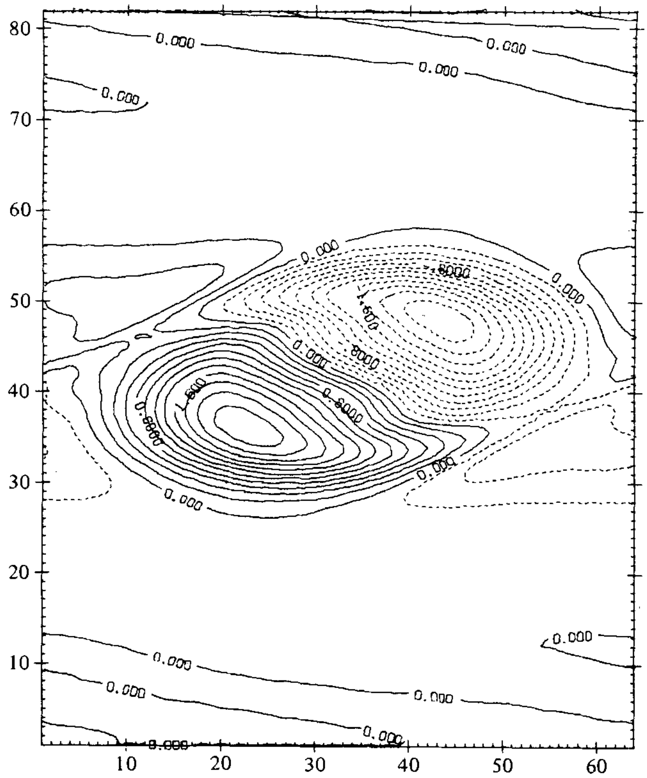

FIGURE 12. The spanwise-periodic perturbation of Ω. Contours of constant values of the perturbations in the (x, z)-plane; case 2, $\tau = 2.5$.

Since the magnitude of $|\boldsymbol{u}|$ depends almost linearly and the Reynolds stresses quadratically on the initial amplitude of the three-dimensional eigenfunctions, it is important to ensure that these are large enough to yield representative three-dimensional motions. This requirement seems to be satisfied at least for case 10 and for $\tau > 2.0$. For this case, the *average* kinetic energy of the three-dimensional perturbation over a domain of height = (1.25 × the grid length) is $0.0028\Delta U^2$, where $\Delta U = 2U_\infty$. The local maximum value of $e_3 = 0.088$, the maximum value of $v = 0.22\Delta U$, which is comparable to the experimental values (e.g. Wygnanski & Fiedler 1970). *Pr* is large. Even at $\tau = 3.0$, it averages 0.016 units of U^3/λ, while, at $\tau = 2.5$, $Pr \approx 0.024U^3/\lambda$. At these rates it would take four to seven units of time τ to transfer to the three-dimensional motion an amount of energy equal to that of the base flow. At $\tau = 3.0$, the maximum value of $|\omega_2| = 5.5$, that of $|\tilde{\omega}| = 7.8$, while that of Ω is 8.0.

4.1. *The effect of the interaction on the spanwise-averaged properties*

Figures 15(*a–c*) compare the spanwise-averaged vorticity $\overline{\Omega}$ for the three cases for $\tau = 3.0$. It is seen that the equivorticity contours for cases 7 and 9 can hardly be distinguished. For case 10 some differences occur: the braids are somewhat wider and slightly asymmetric; in the cores there are several vorticity maxima; the highest value of the average spanwise vorticity does not occur quite at the same pair of points as in case (7), but inward of these, nearer the centre of the figure. But these minor changes do not affect the dynamical interaction between the spanwise vortices and

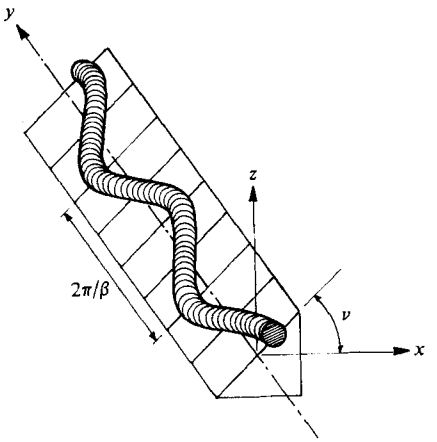

FIGURE 13. Sketch of the periodic displacement of the spanwise vorticity $\Omega+\omega_2$. The angle ν increases with the ratio β/α.

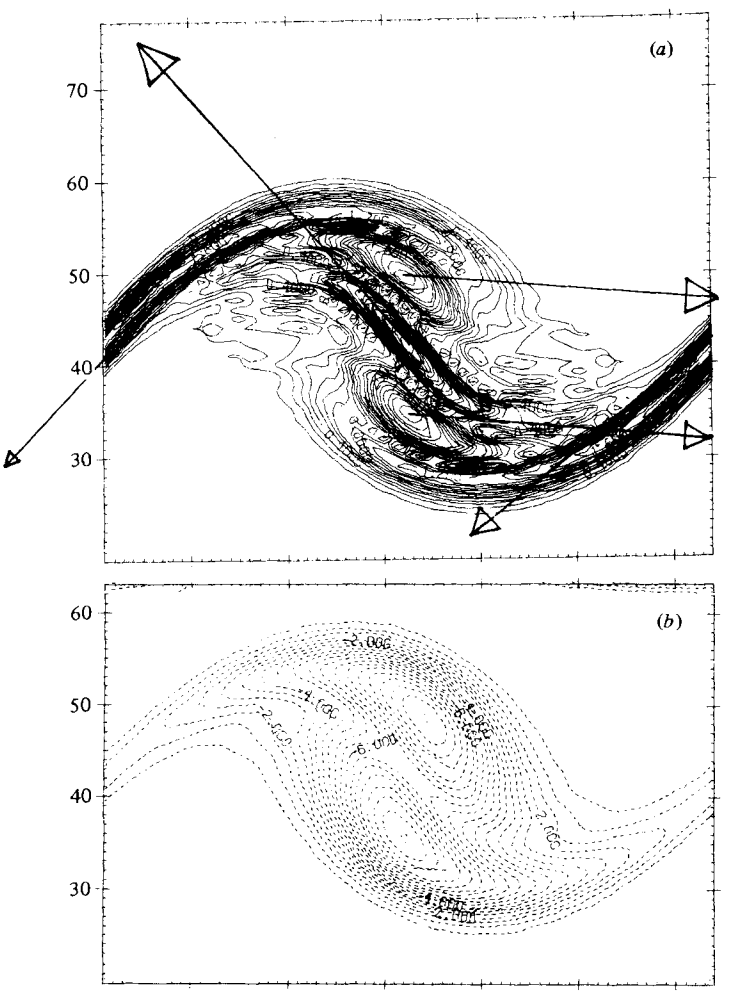

FIGURE 14. (*a*) Magnitude of the streamwise vorticity $\tilde{\omega}$, roll-up and pairing; case 7, $\tau = 3.0$. (*b*) The spanwise vorticity Ω of the base flow at the same time.

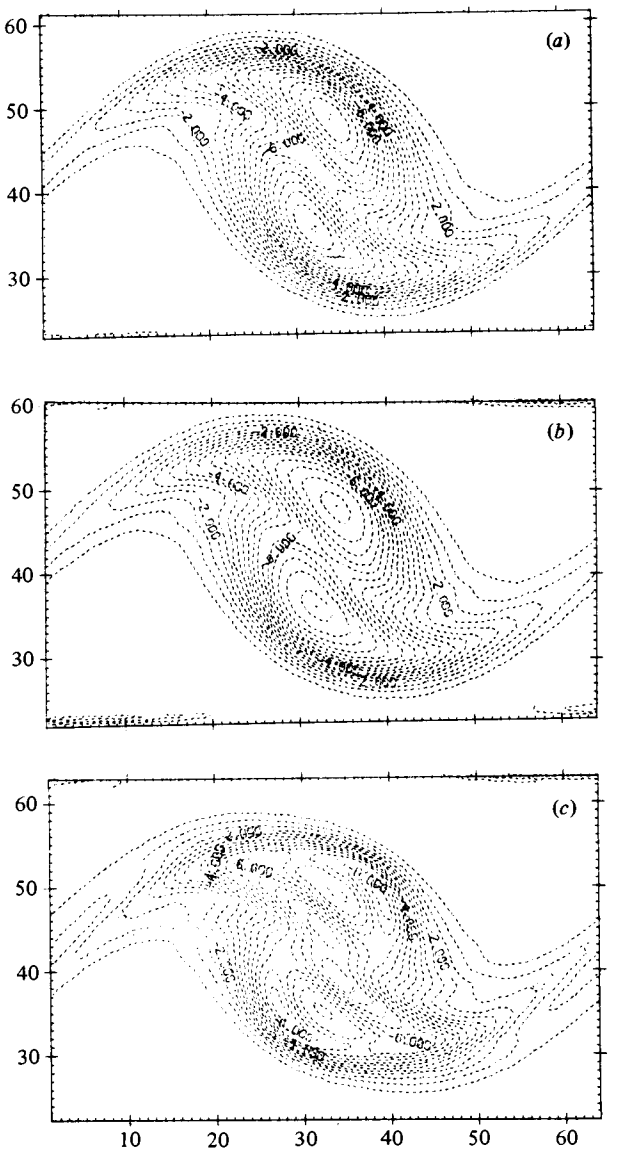

FIGURE 15. Comparison of the spanwise averaged vorticity: (*a*) case 7 (no coupling); (*b*) 9; (*c*) 10.

their coalescence: the pairing process occurs according to precisely the same timescale in all three cases. This is easily seen by plotting the angle θ made by the line joining the two pairing vortices with the x-axis as a function of time. This clockwise-rotating line can be viewed as a clock for the pairing. The plot of θ on figure 16 shows how very nearly identical the pairing history is in all three cases. For comparison, the effect on the clock of doubling the Reynolds number of the initial flow without interaction, shown on the same figure, is far more substantial.†

In fact, none of the integrated measures of the progression of the spanwise-averaged

† It can be seen on the figure that most of this effect occurs during roll-up.

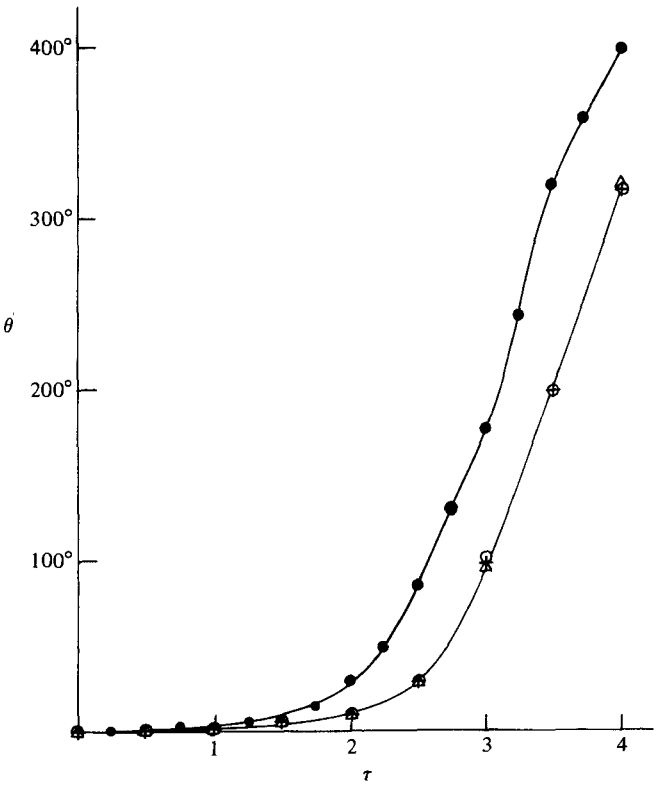

FIGURE 16. The pairing clock: angle θ between line joining the two spanwise vortex centres and the x-axis as a function of time: +, case 7; ○, 9; △, 10; ● is a purely two-dimensional case like (7) but with $R = 100$.

base flow are seriously affected by the vigorous three-dimensional motion. For instance, the cat's-eyes are virtually identical at the same time; the history of the base-flow kinetic energy compared on figure 17 is very nearly so.

The spanwise vorticity distribution $\Omega + \omega_2$ for case 10 is shown at $\tau = 3.5$ on figure 18 for an (x, z)-plane on which the amplitude of ω_2 is maximal.

Our calculations thus give evidence that the base-flow sequential subharmonic instability and the resulting coalescence are quite robust.

It should be noted that the initial conditions used have excluded the case of very strong and purely three-dimensional initial perturbations. These might lead to a very different kind of flow, since they would not provide the environment for a two-dimensional roll-up, and therefore neither pairing nor translative instabilities would follow. In §5 we briefly report another calculation in which the initial perturbations are both indiscriminate and very large. We should also recall a striking experiment carried out by Breidenthal (1980) in which large spanwise perturbations were provided at the origin of a mixing layer by cutting a two-dimensional bevelled trailing edge so that the platform formed a square wave with a spanwise alternation of blunt bases and sharp trailing edges. The visualization of the mixed zone (by the optically visible product of a diffusion-controlled reaction between the two merging streams) revealed that, a few spanwise wavelengths downstream, the mixing layer recovered an essentially two-dimensional pairing structure. By contrast, when the velocity of the two merging streams was the same, the resulting wake was such that the spanwise

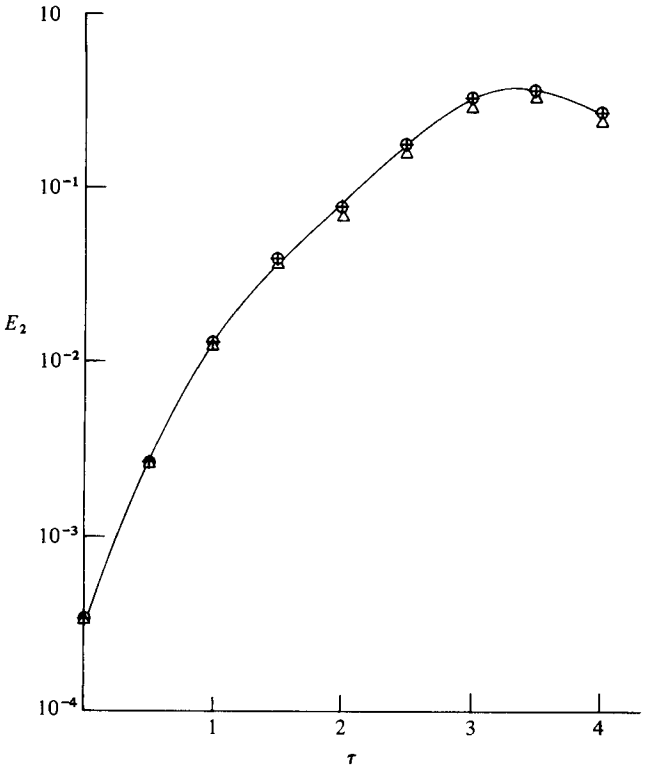

FIGURE 17. The kinetic energy of the spanwise-averaged flow as a function of time: + and curve, case 7; ○, 9; △, 10.

structure imposed by the trailing edge survived with very little lateral transport throughout the visible length of the wake. Such observations cannot be accounted for by the calculations which we have presented. But the specific properties of pairing flows help explain why once the pairing instability is established it is only slightly affected by three-dimensional rivals. The most direct argument can be cast without reference to momentum or energy exchange:

The vorticity equation that corresponds to (2.2*b*) and whose solution is shown in figures 15(*b*, *c*) is

$$\left(\frac{\partial}{\partial t}+\boldsymbol{U}\cdot\boldsymbol{\nabla}-\nu\nabla^2\right)\Omega=\overline{\omega_2\,\partial v/\partial y}+\overline{\tilde{\boldsymbol{\omega}}\cdot\boldsymbol{\nabla}v}-\overline{\boldsymbol{u}\cdot\boldsymbol{\nabla}\omega_2}, \tag{4.1}$$

where overbars denote spanwise averages. Now it has already been both argued and demonstrated from the numerical calculations that, in the intense field of strain created by Ω around the stagnation points, the only component of vorticity that can survive in time is that which is aligned with the direction of positive strain. Thus ω_2 is essentially negligible in the braid region after the latter have formed, so that the first and last terms on the right-hand side of (4.1) are very small. Additionally, the surviving component of vorticity, as we have seen (figures 11*b*, 14*a*) has a direction and a strength which vary little with distance along the braid. This braid (streamwise) vorticity is the main contributor to the local value of v. Thus v varies little with distance along the axis of the braid, so that the last remaining term $\tilde{\boldsymbol{\omega}}\cdot\boldsymbol{\nabla}v$ on the right of (4.1) is likely to be small also. So the interaction terms offer no

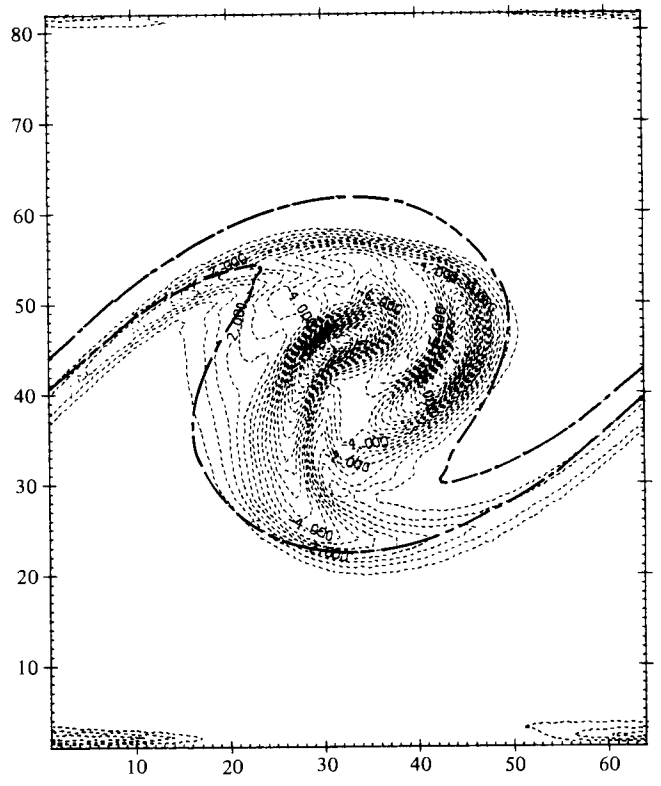

FIGURE 18. The spanwise vorticity $\Omega+\omega_2$ at $y=0$ for case 10 at $\tau=3.5$. The heavy broken line is the outline of the Ω-distribution in the uncoupled case.

mechanism to renew the spanwise vorticity in the depleted braids. These terms are then all confined to the part of the mixing layer that in their absence would contain a substantial amount of spanwise vorticity. Furthermore, these are divergence terms; they can be rewritten as

$$\frac{\beta}{2\pi}\int_0^{2\pi/\beta}\{\tilde{\boldsymbol{\nabla}}\cdot(\boldsymbol{v}\tilde{\omega})+\tilde{\boldsymbol{\nabla}}\cdot(\omega_2\tilde{\boldsymbol{u}})\}\,\delta y,$$

where $\tilde{\boldsymbol{\nabla}}=\hat{\boldsymbol{e}}_x\partial/\partial x+\hat{\boldsymbol{e}}_z\partial/\partial z$, so that their integral over the grid plane (x,z) vanishes. Therefore within the confines of the core they merely transport the existing spanwise vorticity. It is inevitable that such transport aided by molecular diffusion and smaller scales of motion will render the distribution more uniform, thus decreasing somewhat the energy of the base flow, but since it alters neither the circulation nor the size of the spanwise vortices, it should perhaps be expected, that this spatially limited amount of turbulent-like diffusion does not affect the global dynamics of the interacting streamwise vortices.

4.2. *The effect of the coupling on the three-dimensional field*

It can be anticipated that the very modest alterations of the spanwise-averaged properties of the flow which occur in cases 9 and 10 lead only to small changes in the $\boldsymbol{u}$-field. This is indeed the case. Figure 19 shows the ratio of E_3 to its initial value for cases 7, 9 and 10, and figure 20 is a plot of the circulation around the braids at the stagnation points for the same cases. (The loop is rectangular with a span $=2\pi/\beta$.) Contour plots of ω_2, $|\tilde{\boldsymbol{\omega}}|$, p_r and e_3 are similarly almost identical.

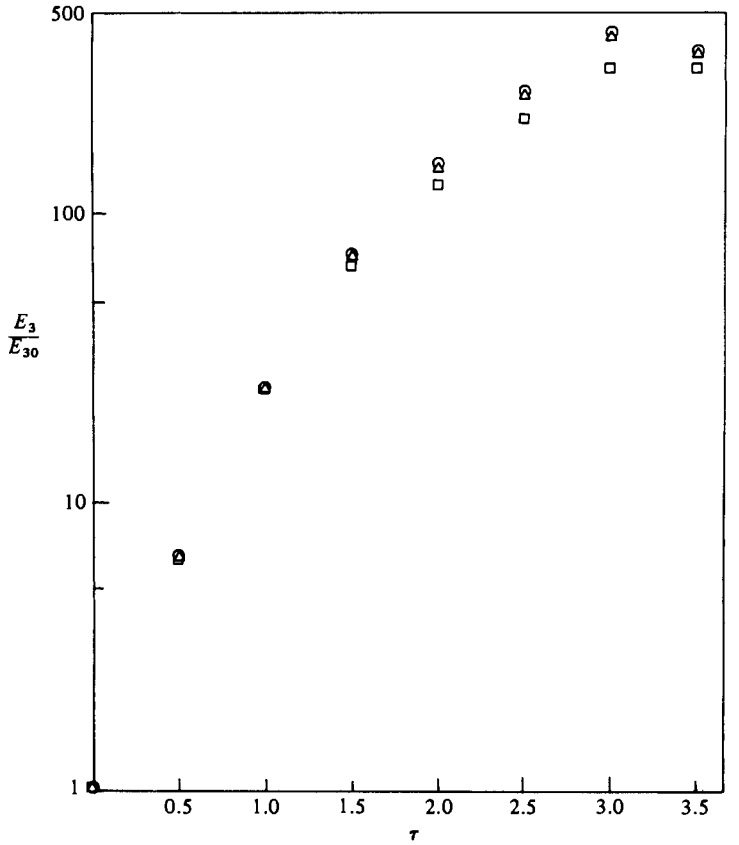

FIGURE 19. Normalized value of E_3 for cases 7 (○), 9 (△) and 10 (□).

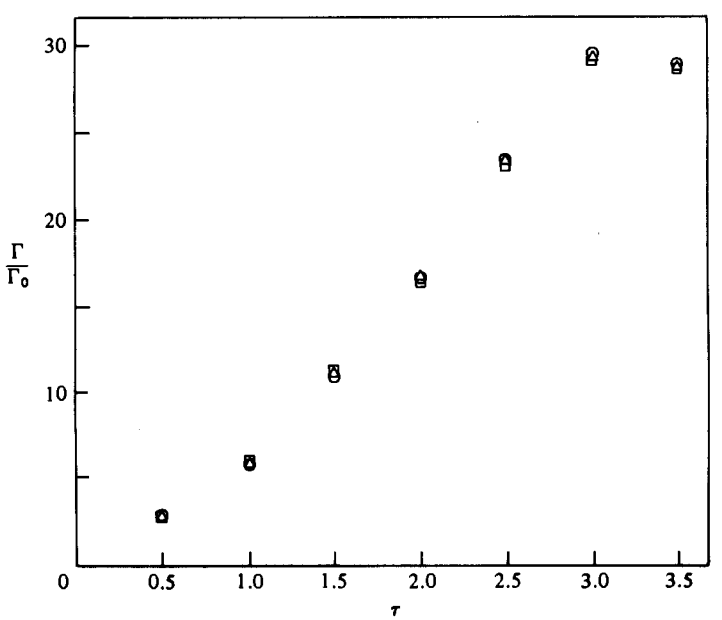

FIGURE 20. The value of the circulation Γ around the braid. For cases 7, 9 and 10, normalized by the circulation Γ_0 at $\tau = 0$.

5. Discussion of other simulations

Four numerical studies of the three-dimensional development of a mixing layer have been reported recently by Riley & Metcalfe (1980), Cain, Reynolds & Ferziger (1981), Couët & Leonard (1980) and Brachet & Orszag (1982).

Riley & Metcalfe and Cain *et al.* use similar pseudospectral methods and initial conditions in a simulation of a turbulent mixing layer. They decompose the velocity field into normal modes in x and y and allow a relatively large number of modes. The initial conditions assign an amplitude distribution in wavenumber space which is a discrete version of a chosen spectrum, shape the distribution in z to simulate a realistic field of turbulence in a shear flow, and assign random phases to the spectral components while insuring that the initial field is solenoidal.

In addition Cain *et al.* provide in general both an eddy-viscosity model and a low-pass filter. The initial amplitude level is very high in Riley & Metcalfe and varies in Cain *et al.* The Reynolds number in Cain *et al.* is 15 in our notation, i.e. low enough (see Corcos & Sherman 1976) to affect seriously the roll-up amplitude and timescale. Because the emphasis was on the simulation of the statistical properties of a turbulent layer, few details of the realizations are given. In Cain *et al.* they consist in the distribution in the (x, z)- and (x, y)-planes of identified particles initially located on the mesh points of a coarse grid in the plane $z = 0$. In Riley & Metcalfe contours of constant spanwise vorticity are given at three times in two (x, z)-planes separated in the y-direction by half a grid length; in spite of the very large initial perturbation amplitudes, in a short time of the order of $\tau = 1.2$, the contours of a characteristic roll-up appear. These contours are somewhat different at the two spanwise stations, though the location of the braids and of the cores are nearly the same. The maxima in the core seem to be displaced up and to the right, down and to the left, much as in our simulation with a single spanwise wavenumber. The length of the grid did not allow pairing.

Couët & Leonard employ a different method which makes use of a large number of initially spanwise vortex filaments with finite vortex cores and whose configurations are defined by the location at any time of 64 initially equidistant nodes along each vortex. The boundary conditions are periodic in x and y. The velocity is calculated from a Poisson equation after the vorticity attached to the filaments has been distributed by a smoothing algorithm within cubic cells (vortex-in-cell methods). A random initial lateral displacement of the filaments is prescribed. While viscosity is ignored in the Helmholtz equation, the vortex-in-cell method should be expected to introduce some numerical diffusion. Some useful inferences can be made from the published results and from a few additional graphical displays.†

The figures consist of:

(*a*) the intersections with the central (x, z)-plane at various times of the vortices that originally belonged to a single row;

(*b*) the projection on to the (x, y)-plane of nodes of the vortices originally uniformly distributed in that plane; and

(*c*) contours in the (y, z)-plane of x- and z-components of the streamwise vorticity $\tilde{\omega}$.

The sideviews in the (x, z)-plane of the vortices indicate that a characteristic roll-up and the initiation of pairing both occur. The shape of the cores is similar to the outline of the spanwise vorticity distribution $\omega_2 + \Omega$ in our calculations. The braids between

† Kindly provided by A. Leonard.

the two main spanwise vortex cores rapidly lose vorticity and become very thin, which suggests that the velocity field induced by the streamwise vorticity is weak next to the velocity induced by the main spanwise vortices in the same region. The contours across the braid of streamwise vorticity projections on to the (y, x)- and (z, z)-planes show that the clockwise and counterclockwise vortices are nearly aligned, suggesting again that their circulation is moderate. This circulation increases rapidly during the early part of the calculation, and seems to level out later. The projection on to the (x, y)-plane of the nodes initially placed there shows a quasi-periodic distortion of the boundaries of the regions of accumulation which resembles Breidenthal's (1981) 'wiggle'. The interpretation of these patterns (and *a fortiori* of the much sparser grid-particle patterns of Cain *et al.*) as the outline of the core is not straightforward and may be seriously misleading. Similarly, the quasi-periodic oscillation of the concentration trace in Breidenthal's (1981) experiment is clearly not an indication that the flow is losing its basic two-dimensionality. However, these node or marker projections give an idea of the typical spanwise wavenumber β which seems to change little with time. In Couët & Leonard $\beta/\alpha_2^{(1)} \approx 3$, while in Cain *et al.* $\beta/\alpha_2^{(1)} \approx \frac{1}{3}$.

In Brachet & Orszag (1982), which came to our attention after this work was completed, pseudospectral methods are used to study in particular the translative instability discovered by Pierrehumbert & Widnall. The initial conditions, like ours, include only one or two two-dimensional modes and a single three-dimensional one. But the authors investigated a larger range of values of β. In their calculations the initial amplitude of the two-dimensional fundamental mode was always several orders of magnitude larger than that of the other two perturbations, and in all cases but one the subharmonic amplitude was either zero or several orders of magnitude smaller than that of the three-dimensional mode. Thus the object of the study was primarily the three-dimensional evolution of a layer that rolls up early and is essentially constrained not to pair. The results are therefore comparable to those for our cases 1–4.

The authors find that the translational instability is approximately exponential and gives no sign of saturation or equilibration as the three-dimensional motion becomes large. They conclude that chaos results. They find that for $\beta > 2$ the growth rate of the energy of the three-dimensional motion is a steadily decreasing function of β for α_3 and R fixed. They suggest that for $\alpha_2 = \alpha_3 = 0.4$ the three-dimensional flow becomes stable for $\beta > \beta_{\text{critical}} \approx \frac{1}{3}R^{\frac{1}{2}}$. They find that the growth rate of the subharmonic (measured by the energy residing in the mode $\alpha_2^{(2)}$ alone) is greater than that associated with the modes of the three-dimensional motion. Finally their results indicate that, even when the initial energy of the three-dimensional motion is 10^5 times larger than that of the subharmonic, the subharmonic growth rate is nearly unaffected by the development of the three-dimensional motion ($Re = 400$, $\alpha_2^{(1)} = 0.4$, $\beta/\alpha_3 = 0.5$).

These results supplement ours usefully and are consistent with them. One should note that only in the absence of a subharmonic of competitive initial amplitude do the computations in Brachet & Orszag lead to a progressive disorganization of the two-dimensional flow whose own instability has been arrested. It is very unlikely that a naturally perturbed layer would be provided exclusively with a single two-dimensional mode of disturbance (required for roll-up and therefore for translative instability) together with three-dimensional modes (required for the translative instability) without modes suitable for seeding of the faster-growing pairing instability.

6. Conclusions

It was the hypothesis of Part 1 that in the mixing layer there exists a hierarchy of motions, of which the primary and controlling one is closely given by two-dimensional solutions of the equations of motion. Parts 1 and 2 have shown that while the initial instability of parallel shear flow, the well-known Orr–Sommerfeld instability, causes the growth of both two- and three-dimensional disturbances (with a selectively greater growth rate for the more-nearly two-dimensional disturbances), this instability gives way to two distinctly different other types. The first, preferentially two-dimensional, is the sequential pairing instability, which causes the growth of the layer by the coalescence of spanwise vortices. The second, preferentially three-dimensional and discovered by Pierrehumbert & Widnall, can be expected to grow side by side with the pairing instability, but is both slower-growing and inhibited by the latter, at least through one pairing. That instability is strongly centred in the spanwise vortex cores. Thus it is likely that the strong streamwise vorticity that appears and persists in the central part of the braids, and which is responsible for the streamwise streaks in Bernal *et al.* (1980), is caused early on by the original (three-dimensional) shear instability rather than by the translative instability, and thereafter leads a fossil life.†

One may surmise that, since the two-dimensional growth through successive pairings (which halve the value of α) is linear on the average, while the growth rate of the translative waves, even if we ignore the effect that pairing has on them, falls off progressively with increasing values of β/α, the three-dimensional motion that results from this type of flow should not succeed in altering the fundamental two-dimensional pairing mechanism through which the layer grows and which sustains all other modes and scales of motion.

It should be noted that neither our calculations nor any other calculation or analysis reported so far give a good idea of a typical spanwise scale of, say, streamwise vorticity, or explain what determines that scale, since the weak filter offered by parallel-flow analysis is replaced later by an even broader filter as our work and that of Brachet & Orszag (1983) show. Either nonlinear interaction of waves of neighbouring spanwise wavenumber (particularly difficult to study numerically over a finite domain) or the competitive advantage given by particular initial conditions may lead to a selective mechanism.

This work has been supported by the U.S. Office of Naval Research under contract N.R. 062-665.

† It seems paradoxical, as noted by a referee, that in those experiments the most clearly observed features of the three-dimensional instability should not be associated with the most-energetic manifestations of this instability. But the success of the visualization method used depends on a nonlinear feature of streamwise vorticity layers: their propensity to become concentrated into strong almost axially symmetric, vortices when they are stretched. This is discussed and illustrated in detail in Part 3 (Lin & Corcos 1984). Thus the visual contrast is a much more sensitive index of the intensity of the local gradients of streamwise vorticity than it is of its circulation or of the energy associated with it. In addition, the projection onto planes of the concentration-gradient-related optical contrast may give poor resolution, i.e. partial integration of gradients in convoluted regions such as the cores.

REFERENCES

BENNEY, D. J. 1961 *J. Fluid Mech.* **10**, 209.

BERNAL, L. P. 1981 The coherent structure of turbulent mixing layers. I. Similarity of the primary structure. II. Secondary streamwise vortex structure. Ph.D. thesis, Calif. Inst. of Tech.

BERNAL, L. P., BREIDENTHAL, R. E., BROWN, G. L., KONRAD, J. H. & ROSHKO, A. 1980 In *Turbulent Shear Flows 2* (ed. L. J. S. Bradbury, F. Durst, B. E. Launder, F. W. Schmidt & J. H. Whitelaw), p. 305. Springer.

BRACHET, M. E. & ORSZAG, S. 1982 Secondary instability of free shear layer flows. Preprint submitted for publication.

BREIDENTHAL, R. 1980 *Phys. Fluids* **23**, 1929.

BREIDENTHAL, R. 1981 *J. Fluid Mech.* **109**, 1.

CAIN, A. B., REYNOLDS, W. C. & FERZIGER, J. H. 1981 A three-dimensional simulation of transition and early turbulence in a time-developing mixing layer. *Stanford Univ. Dept. Mech. Engng Rep.* TF-14.

CORCOS, G. M. 1979 The mixing layer: deterministic models of a turbulent flow. *Univ. Calif., Berkeley, Coll. Engng Rep.* FM-79-2a.

CORCOS, G. M. & SHERMAN, F. S. 1976 *J. Fluid Mech.* **73**, 241.

CORCOS, G. M. & SHERMAN, F. S. 1984 *J. Fluid Mech.* **139**, 29.

COUËT, B. & LEONARD, A. 1980 Mixing layer simulation by an improved three-dimensional vortex-in-cell algorithm. In *Proc. 7th Intl Conf. on Numerical Methods in Fluid Dynamics, Stanford–Ames.*

KONRAD, D. H. 1977 An experimental investigation of mixing in two-dimensional turbulent shear flows with applications to diffusion-limited chemical reactions. Ph.D. thesis, Calif. Inst. of Tech. (Also *Project Squid Tech. Rep.* CIT-8-PU, Dec. 1976.)

LIEPMANN, H. W. & LAUFER, J. 1949 Investigation of free turbulent mixing. *NACA TN* 1257.

LIN, S. J. & CORCOS, G. M. 1984 The mixing layer: deterministic models of a turbulent flow: Part 3. The effect of plane strain on the dynamics of streamwise vortices. *J. Fluid Mech.* (to be published).

PIERREHUMBERT, R. T. & WIDNALL, S. E. 1982 *J. Fluid Mech.* **114**, 59.

RILEY, J. J. & METCALFE, R. W. 1980 Direct numerical simulation of a perturbed turbulent mixing layer. *AIAA 18th Aerospace Sciences Meeting, Pasadena, CA: AIAA Reprint* 080-0274.

STUART, J. T. 1963 In *Laminar Boundary Layers* (ed. L. Rosenhead), chap. 9, §4. Oxford University Press.

STUART, J. T. 1967 *J. Fluid Mech.* **29**, 417.

WYGNANSKI, I. J. & FIEDLER, H. E. 1969 *J. Fluid Mech.* **38**, 577.